The Journal of Chemical Physics ARTICLE pubs.aip.org/aip/jcp

# Non-covalent interactions in conjugated polymer blends: Insights into the stability of PVC/PM6 and CPE/PM6 systems

Cite as: J. Chem. Phys. 161, 214902 (2024); doi: 10.1063/5.0239969
Submitted: 23 September 2024 • Accepted: 18 November 2024 •
Published Online: 3 December 2024



Ram Sewak, Rudranarayan Khatua, and Anirban Mondal[a]

## AFFILIATIONS

Department of Chemistry, Indian Institute of Technology Gandhinagar, Gujarat 382355, India

**Note:** This paper is part of the JCP Special Topic on Molecular Dynamics, Methods and Applications 60 Years After Rahman.
[a]**Author to whom correspondence should be addressed:** amondal@iitgn.ac.in

## ABSTRACT

This study investigates the role of non-covalent interactions (NCIs) in stabilizing blends of the conjugated polymer PM6 with additives polyvinyl chloride (PVC) and chlorinated polyethylene (CPE). Using the NCI index, reduced density gradient analysis, and energy decomposition analysis (EDA), we quantify the contributions of van der Waals forces, hydrogen bonding, and steric repulsions in these systems. Our results reveal that PVC/PM6 blends exhibit stronger NCI, particularly C–H$\cdots\pi$ and C–Cl$\cdots\pi$ interactions, compared to CPE/PM6 blends. EDA further shows that dispersion forces and electrostatic interactions are the primary stabilizing factors in the PVC blend, with hydrogen bonding also playing a critical role. These findings highlight the importance of chlorine content in enhancing NCI and promoting the stability of polymer blends. The insights from this work provide valuable guidance for designing more stable polymer-additive systems in organic electronics and other material applications.





## I. INTRODUCTION

Conjugated donor/acceptor polymers have emerged as promising candidates for flexible and wearable electronic devices owing to their low cost, mechanical flexibility, intrinsic semiconducting properties, and efficient charge separation capabilities. These polymers play a pivotal role in various flexible components, including organic light-emitting diodes (OLEDs), organic field-effect transistors (OFETs), and organic solar cells (OSCs).[1] Despite their potential, the degradation of these materials—whether due to chemical, morphological, or mechanical pathways—poses a substantial barrier to their widespread commercial application.[2,3]

Various strategies have been explored to address these challenges and enhance the mechanical properties of conjugated polymers used in OSCs and OFETs. One notable approach involves incorporating insulating polymers into conjugated polymers to improve flexibility. However, the poor miscibility between these two types of polymers often limits the effectiveness of this strategy.[4,5] To overcome this limitation, carboxylation of insulating polymers has been shown to enhance their miscibility with conjugated polymers, leading to significantly improved mechanical properties and higher crack-onset strains.[6] Nevertheless, introducing insulating polymers can adversely affect electron mobilities and power conversion efficiencies in photoactive layers, underscoring the need for carefully selecting polymers that promote strong non-covalent interactions (NCIs).[7] Furthermore, selective contact doping with molecules such as 2,3,5,6-tetrafluoro-7,7,8,8-tetracyanoquinodimethane ($F_4$-TCNQ) in conjugated polymers has proven effective in enhancing carrier injection in OFETs, offering potential for scalable and low-power organic devices.[8] Another promising strategy involves incorporating thermoplastic elastomers, such as polystyrene-block-poly(ethylene-ran-butylene)-block-polystyrene (SEBS), to reduce stiffness and enhance stretchability while maintaining high efficiency in OSC blends.[9] These approaches collectively illustrate the ongoing efforts to balance mechanical robustness with electronic performance in flexible organic electronics. Moreover, recent studies have highlighted the significance of non-covalent interactions (NCIs), such as dipole–dipole interactions and hydrogen bonding, in improving the mechanical properties and thermal stability of flexible organic electronics.[5] Thus, the physical mixing of additive

components into conjugated polymers emerges as a promising strategy. This method can exploit non-covalent interactions, including strong hydrogen bonding and $\pi$–$\pi$ interactions at cross-linking sites, particularly with aromatic-pendent polymers.[10–12] In addition, incorporating additive components can reduce the crystallinity of conjugated polymers,[7,13,14] further enhancing the mechanical flexibility of these materials.

While it is well established that these non-covalent interactions significantly influence the morphological and mechanical stability of additive-conjugated polymer blends, there has been limited exploration into how these properties are fundamentally interrelated, both phenomenologically and through their underlying quantitative and qualitative aspects. This gap in understanding raises critical questions about the types of interactions that may arise when mixing such additives and whether these interactions can be theoretically quantified to establish design principles for new materials.

Since non-covalent interactions are driven by partial charges and electron clouds on atoms and molecular rings, they can vary in strength, typically ranging from −0.5 to −50 kcal mol$^{-1}$.[15] Unlike covalent bonds, NCIs do not impart significant rigidity and are relatively easy to form and break.[16,17] Depending on the strength and nature of the interacting atoms or molecules, these interactions can be classified into several categories.[17,18] For example, van der Waals forces represent weak interactions caused by temporary dipoles in molecules, while dipole–dipole interactions occur between molecules with permanent dipoles. Hydrogen bonding, a stronger dipole–dipole interaction, involves hydrogen atoms bonded to electronegative atoms such as oxygen or nitrogen. $\pi$–$\pi$ interactions occur between aromatic rings, contributing to the stability of conjugated systems. In addition, electrostatic interactions result from the attraction between charged species. Each of these interactions contributes uniquely to the overall properties of the blend system, influencing both the mechanical flexibility and stability of the resulting material.

In non-covalent interactions, hydrogen bonds (H-bonds), hydrophobic forces, van der Waals interactions, and steric repulsion are commonly observed, each contributing in varying degrees to the overall interaction strength within a system. These weak forces play a crucial role in determining the miscibility of polymers and additives, as they facilitate the formation of intermolecular connections that promote the clustering of molecules. A clear understanding of these interactions is essential for predicting the behavior of blended materials. Among the various non-covalent interactions, hydrogen bonds are particularly significant due to their strong influence on the structural integrity and blending efficiency of conjugated polymers with additives. These interactions occur between a hydrogen atom attached to an electronegative donor atom (D) and an acceptor atom (A), which is also electronegative. The strength of hydrogen bonds can vary widely, largely depending on the nature of the donor and acceptor atoms as well as the surrounding environment. In some cases, H-bonds can be as strong as −40 kcal mol$^{-1}$,[19] although they can also be much weaker, such as the C–H···O interactions commonly observed in organic systems. Hydrogen bonds are generally categorized by their strength: conventional H-bonds, ranging from −2.4 to −12.0 kcal mol$^{-1}$; low-barrier H-bonds, with energies between −12 and −24 kcal mol$^{-1}$; and single-well H-bonds, which exceed −24 kcal mol$^{-1}$ in strength.[20] In addition, Jeffrey[21] proposed a classification based on donor–acceptor distances: strong, predominantly covalent bonds at 2.2–2.5 Å; moderate, primarily electrostatic bonds at 2.5–3.2 Å; and weak, electrostatic bonds at 3.2–4.0 Å.

While oxygen and nitrogen are well-known for their roles in hydrogen bonding, the sulfur-mediated H-bonds have traditionally been considered weaker due to the "lower electronegativity" of sulfur. As a result, these interactions are often overlooked. However, studies employing vapor-phase infrared spectroscopy and *ab initio* calculations have revealed that sulfur, although weaker than oxygen, can still serve as an effective hydrogen bond acceptor.[22] Recent research by Chand *et al.*[23] further elucidates the stabilizing effect of sulfur (S) and selenium (Se) in proteins and biomolecules through hydrogen bonding, with bond strengths ranging from 1.4 to 6.6 kcal mol$^{-1}$. Similar studies have identified weak to moderate X–H···Cl hydrogen bonds (X = C, N, O), with binding energies between −2.8 and −5.3 kcal mol$^{-1}$,[24] underscoring the importance of these often underappreciated interactions in determining the overall behavior of complex molecular systems.

In this study, we systematically investigate the various types of non-covalent interactions within a system of PM6 conjugated polymer mixed with the additives polyvinyl chloride (PVC) and chlorinated polyethylene (CPE). By performing molecular simulations at 300 K to replicate real-world conditions, we can closely examine how environmental factors influence these interactions, which are crucial in determining the morphology and properties of conjugated polymers. The selection of PVC and CPE as additives for PM6 was motivated by their unique structural characteristics and experimental relevance. PVC, with its head-to-tail regioregularity, and CPE, with a more irregular structure, both contain chlorine atoms, allowing us to explore the influence of structural order on non-covalent interactions. Notably, experimental studies[5] have shown that adding PVC to PM6 films improves mechanical resilience, as indicated by a higher crack-onset strain attributed to hydrogen bonding and non-covalent interactions. In contrast, CPE did not significantly alter the blend's mechanical properties. These differences provided an opportunity to systematically investigate the distinct non-covalent interactions in PM6/PVC and PM6/CPE blends, addressing a gap in understanding the interplay of weak interactions in conjugated polymer systems.

This work not only sheds light on the underlying mechanisms of non-covalent interactions but also offers valuable insights that can guide experimentalists in understanding the complex morphology of polymer blends. Ultimately, our findings pave the way for the design of novel, robust, and flexible conjugated polymer blends, marking a significant advancement in the field of flexible organic electronics.

## II. METHODS

In this study, we utilized the OPLS-AA force field[25,26] to conduct molecular dynamics (MD) simulations via the GROMACS 2020.4 package.[27,28] The all-atom optimized potentials for liquid simulations (OPLS-AA) force field is well-suited for capturing non-covalent interactions due to its comprehensive parameterization, incorporating 12-6 Lennard-Jones (LJ) and Coulombic potentials for nonbonded interactions, along with detailed parameters for bonded interactions, including bonds, angles, dihedrals, and impropers. Given the critical role of accurately modeled partial atomic charges in reproducing experimental properties, we

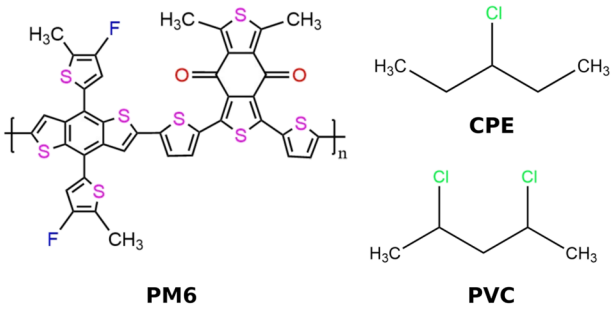


**FIG. 1.** Chemical structures of the monomers PM6, CPE, and PVC.

employed the LigParGen server.[29] This server utilizes the quantum mechanical (QM)-based charge model 1.14*CM1A-LBCC, enhancing the precision of the OPLS-AA force field over its original version, which relied on individual parameterization.[25]

Our simulations focused on blending PM6 conjugated polymers with PVC and CPE additives. The structures of the PM6 monomer, CPE, and PVC are presented in Fig. 1. Conventionally, in PVC and CPE, the two hydrogen atoms attached to the carbon atoms in the middle of the polymer chain are referred to as $\alpha$-H. The single hydrogen atom bonded to a carbon atom that is attached to a chlorine atom is denoted as a $\beta$-H, while the hydrogen atom at the terminal of the chain, associated with a methyl group, is referred to as *m*-H. Throughout the text, this nomenclature will be followed. The initial geometries for PM6, PVC, and CPE were optimized using the B3LYP functional with the Def2SVP basis set in Gaussian09.[30] To set up the blended configurations of PM6/PVC and PM6/CPE, we used Packmol[31] to position 1000 PM6 molecules (each containing two repeat units, totaling 152 atoms per molecule) and ten single-unit PVC or CPE molecules (17 atoms each). A minimum inter-molecular distance of 2 Å was enforced to ensure uniform distribution of the molecules. This setup resulted in 152 170 atoms in the packed configurations, ensuring a comprehensive and realistic model for exploring non-covalent interactions within these blended systems. The choice of blending concentration was based on the experimental conditions reported in Ref. 5, which utilized a 1 wt. % concentration of additives. This concentration allowed us to maintain adequate dilution for computational efficiency while simulating conditions relevant to experimental observations.

We employed a temperature annealing process within the *NpT* ensemble to achieve optimal miscibility and replicate real-world processing conditions. These simulations were performed using a canonical velocity rescaling thermostat,[32] a Berendsen barostat for pressure coupling,[33] and the smooth particle mesh Ewald technique for long-range electrostatic interactions. The system was heated from 100 to 800 K over 3 ns, allowing the components to mix thoroughly. Before annealing, energy minimization was conducted using the steepest-descent method to relax the initial structures. Following the annealing, we implemented a cooling phase in two stages: from 800 to 600 K and then from 600 to 300 K, with both steps performed under the *NpT* ensemble over an additional 3 ns. This gradual cooling process was crucial for stabilizing the system's morphology. After completing the cooling process, we carried out 3 ns production runs in the *NVT* ensemble at 300 K to capture the system's dynamic behavior under standard conditions. The total simulation time of 3 ns was chosen based on equilibration monitoring, which showed stable thermodynamic parameters (e.g., temperature, pressure, and potential energy) and consistent radial distribution functions (RDFs) over the last nanosecond. These indicators suggest that 3 ns was adequate for reaching equilibrium in this system. The Verlet leapfrog algorithm was employed to integrate equations of motion with a time step of 1 fs.[34] Non-bonded interactions were computed with a real space cutoff of 1.3 nm. The trajectories obtained from these simulations were visualized using visual molecular dynamics (VMD)[35] to gain initial insights into the weak interactions between interatomic pairs.

To accurately identify regions of non-covalent interactions within the polymer-additive systems, we employed the NCIPLOT4 package.[36] This tool is particularly effective in detecting weak interaction regions within chemical systems by analyzing the electron density $\rho(r)$ and its derivatives. When weak inter- or intramolecular interactions occur between the fragments of the system, critical density points arise between the interacting components.[37] These points induce significant changes in the reduced density gradient (RDG), a dimensionless function that normalizes the electron density gradient, effectively highlighting regions of weak interaction. The RDG is calculated using the following equation:

$$\mathrm{RDG}(r) = \frac{1}{2(3\pi^2)^{1/3}} \frac{|\nabla\rho(r)|}{\rho^{4/3}}. \tag{1}$$

Given that the RDG is particularly sensitive in low-density regions, it approaches zero near the critical points where the electron density gradient ($\nabla\rho$) becomes predominant. This sensitivity results in the identification of troughs within the RDG, corresponding to weak interaction regions.[37] The electron density employed in this method is derived from promolecular estimates. This approach avoids the electronic relaxation typically introduced in the self-consistent field (SCF), such as Hartree–Fock or density functional theory (DFT) calculations. Consequently, this method offers a computationally efficient alternative for large systems while still providing NCI insights comparable to those obtained from more computationally intensive SCF methods.

To quantitatively evaluate the contributions of various weak interaction energies, energy decomposition analysis based on the classical molecular force field (EDA-FF) was conducted using the Multiwfn package.[38] This approach provides detailed insights into interatomic and interfragment interactions based on molecular force fields. For the energy decomposition analysis, randomly, 500 polymer-additive dimer pairs of PM6 and PVC/CPE were selected within a cutoff distance of 6 Å from the production simulation trajectory. In the context of weak interactions, the primary components are van der Waals (vdW) interactions and electrostatic interactions. These interactions can be described using pairwise potentials. In the EDA-FF framework, the vdW interaction is computed using the standard Lennard-Jones 12-6 potential, as expressed in the following equation:

$$V(r) = 4\epsilon\left[\left(\frac{\sigma}{r}\right)^{12} - \left(\frac{\sigma}{r}\right)^{6}\right]. \tag{2}$$

To further refine our analysis and calculate the precise contribution of non-covalent interaction energies, we utilized

quantum mechanical (QM) methods, specifically symmetry-adapted perturbation theory (SAPT), implemented within the Psi4 1.1 package.[39] Due to the high computational cost associated with analyzing a complete dimer configuration comprising two PM6 monomers and one CPE/PVC molecule, we opted for an alternative approach. We selected a simplified dimer configuration involving a single PM6 molecule paired with one CPE or PVC molecule. We performed SAPT calculations on these individual pairs, considering only one configuration for each polymer blend. These configurations were optimized using ground-state DFT prior to SAPT0 calculations (suitable for open-shell monomers).[40] We employed the B3LYP/6-31+g(d,p) method for these calculations as implemented in the Gaussian 09 package,[30] including polarization and diffuse functions to ensure an accurate representation of electron distributions. All calculations within Psi4 utilized density fitting techniques in both SCF and post-SCF methods, with the frozen core approximation applied to simplify the chemical core, ensuring computational efficiency while maintaining accuracy.

## III. RESULTS AND DISCUSSION

In this study, we employed the OPLS-AA force field, which has been widely used in modeling organic electronic materials and polymer systems, to balance computational efficiency and accuracy in capturing non-covalent interactions.[41–44] To validate the suitability of OPLS-AA for our system, we compared the dipole moments of gas-phase dimer pairs (PM6+CPE and PM6+PVC) and individual molecules calculated with OPLS-AA against DFT-calculated values. The dipole moment of PM6+CPE calculated with OPLS-AA was 2.13 D, closely matching the DFT value of 2.2 D, while for PM6+PVC, the OPLS-AA result was 5.44 D, in good agreement with the DFT-calculated 5.02 D. Similarly, for individual molecules, the dipole moments calculated with OPLS-AA and DFT showed good consistency: for PVC, 3.17 (OPLS-AA) vs 3.48 D (DFT); for PM6, 2.75 (OPLS-AA) vs 2.20 D (DFT); and for CPE, 3.0 (OPLS-AA) vs 2.29 D (DFT). These results reinforce the suitability of the OPLS-AA force field in accurately modeling electrostatic properties for the PM6 blends in our study.

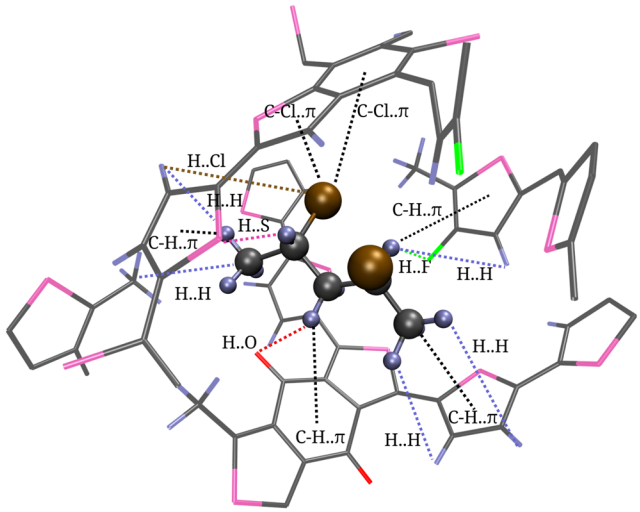


**FIG. 2.** Representation of different types of weak interactions around PVC molecules in PM6–PVC blends through VMD software.[35] Color scheme: carbon: gray, hydrogen: iceblue, oxygen: red, chlorine: brown, sulfur: pink, and fluorine: light green.

### A. Interaction via hydrogen bonds

To explore the hydrogen bonding interactions within the PM6–PVC and PM6–CPE blends, we began by visualizing the clustering of PM6 molecules around PVC and CPE. This initial visualization allowed us to identify potential interactions based on distance criteria, highlighting the presence of hydrogen bonds between various atoms of PM6 (such as O, F, and S) and the $\alpha$-, $\beta$-, and $m$-H atoms of PVC and CPE, as illustrated in Fig. 2. An analysis of the average distance profile for weak interactions was carried out using the radial distribution function (RDF). Figures 3(a)–3(c) present RDF plots showing the interactions between the $\alpha$, $\beta$, and methyl hydrogens of CPE/PVC and the oxygen atoms of the carbonyl groups in the six-membered rings of PM6. The first peak in the RDF, which corresponds to hydrogen bonds between the $m$-H of PVC and the oxygen atoms in PM6, appears at around 2.7 Å in the PM6/PVC mixture [Fig. 3(a)]. In contrast,

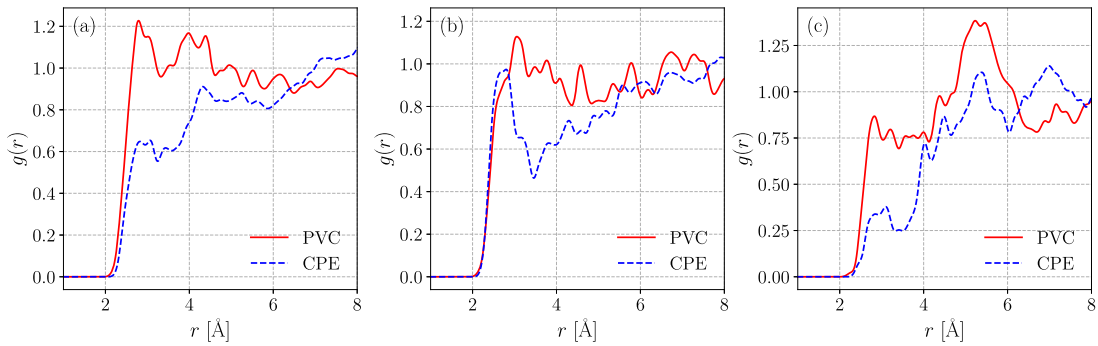


**FIG. 3.** Radial distribution functions between oxygen atoms of the carbonyl groups present in the six-member ring of PM6 and (a) methyl ($m$-), (b) $\alpha$–, and (c) $\beta$–H of CPE and PVC molecules.

the CPE mixture shows a slight shift, indicating weaker hydrogen bonding, with roughly half the number of hydrogen bonds as the PVC mixture, as reflected in the lower peak height. A similar pattern is observed for the $\beta$-H and oxygen interaction in Fig. 3(c), although the probability of this interaction is lower compared to the $m$-H bond. Interestingly, the $\alpha$-H and oxygen interaction in the CPE mixture exhibits a short-distance prominent peak at 2.7 Å, as shown in Fig. 3(b). In comparison, the corresponding interaction in the PVC mixture shows a slightly shifted peak at 3 Å; however, with a higher probability, suggesting differences in the nature of the interaction across the two mixtures. The observed $\beta$-H bonding interaction aligns with the findings of Guan *et al.*,[5] who reported similar interactions in PM6/PVC blends, identifying hydrogen bonds between the oxygen atoms of the C=O groups and the $\beta$-hydrogen of PVC through XPS and FTIR spectroscopy. However, they did not detect such interactions in PM6/CPE blends. Our RDF analysis corroborates their conclusion, as the interaction appears stronger in PM6/PVC blends compared to PM6/CPE blends, as evidenced by the more pronounced peak heights in the RDF plots.

In addition, weak hydrogen bonds with an average distance of 3 Å were identified between the chlorine atoms of PVC/CPE and the hydrogens attached to the five-membered rings, as well as the methyl hydrogens of PM6's side chains, as shown in Figs. S1(a)–S1(c) of the supplementary material. The number of hydrogen bonds between chlorine and the methyl hydrogens, along with the single hydrogen attached to the aromatic ring, is more pronounced in the CPE mixture compared to the PVC mixture. Conversely, the hydrogen bonding between chlorine and the two hydrogens attached to aromatic rings is more prevalent in the PVC mixture than in the CPE mixture at the same concentration.

Relatively weak hydrogen bonding is also observed between the hydrogen atoms of PVC/CPE and the fluorine or sulfur atoms in PM6, as shown in Figs. S1(d), S1(e), S1(g), and S1(i). In particular, Fig. S1(f) highlights that the $\beta$-hydrogen in PVC forms a slightly stronger hydrogen bond (around 2.5 Å) with the fluorine atom of PM6, compared to the $\beta$-hydrogen in CPE, where the distance is ~2.7 Å. However, for other hydrogen bonds involving F and S atoms, the RDF reveals broad, diffuse peaks, indicating weaker, less-defined interactions. As a result, the contributions from these hydrogen bonds to the overall non-covalent interactions are minimal and can be considered negligible.

## B. van der Waals interactions

Building on the previous discussion of hydrogen bonding, the van der Waals (vdW) interaction is another critical force contributing to the overall non-covalent interactions in PM6–PVC and PM6–CPE blends. The attractive component in the Lennard-Jones potential [Eq. (2)] stems from quantum mechanical electron correlation effects and represents a non-directional dispersion interaction, commonly called vdW or London dispersion interaction. This interaction is a critical force between non-polar and weakly polar molecules, driven by transient fluctuations in electron density.[45] The strength of vdW interactions depends on the polarizability of the atoms involved, with the energy decreasing proportionally to the sixth power of the distance between them [Eq. (2)].[46,47] As a benchmark, the gas-phase methane dimer ($CH_4 \cdots CH_4$) exhibits an interaction energy of approximately −0.4 kcal mol$^{-1}$,[48] underscoring the significance of such interactions in non-polar systems.

**C–H$\cdots\pi$ interactions:** Among the vdW interactions, the C–H$\cdots\pi$ interaction stands out due to its relevance in systems with aromatic components. This interaction involves a C–H group acting as a donor and the $\pi$-electron cloud of an aromatic ring serving as an acceptor. Although the nature of C–H$\cdots\pi$ interactions is predominantly dispersive, it also shares similarities with hydrogen bonding, especially in highly acidic C–H bonds. The interaction strength typically ranges from −1.5 to −2.5 kcal mol$^{-1}$, comparable to C–H$\cdots$O interactions.[49] These interactions are driven mainly by dispersion and electrostatic forces, with minimal contributions from hydrophobic effects.[49,50]

In our study, strong van der Waals interactions between $\alpha$-H and the $\pi$-cloud of the five-membered bridging rings in PM6 are observed, as reflected by a distinct RDF peak around 3.1 Å in the PVC blend [Fig. 4(a)]. In contrast, the CPE blend shows no prominent peak, suggesting weaker $\pi$-cloud interactions. A similar interaction is seen between $\beta$-H and the $\pi$-cloud, with an RDF peak at 3.2 Å in the PVC blend, whereas in the CPE blend, this peak shifts to 3.0 Å with roughly half the probability [Fig. 4(b)]. Another notable C–H$\cdots\pi$ interaction between $\beta$-H and the methyl-substituted five-membered aromatic ring in the PVC blend is observed at 3.4 Å [Fig. 4(c)]. A peak is absent in the CPE blend.

The strength of these interactions can be attributed to reduced steric hindrance at the intermolecular level, further amplified by the chlorine atoms in PVC/CPE, which results in an enhancement in the electrostatic interaction with hydrogen atoms and thereby strengthens the C–H$\cdots\pi$ bonds. The RDF plots [Figs. 4(d) and 4(e)] show a distinct peak around 3.5 Å in the PVC blend, whereas the corresponding peak in the CPE blend is significantly broadened and of lower probability. This broadening can be attributed to steric effects from positioning the six-membered aromatic ring, which hinders optimal interaction and contributes to the weaker overall attraction.

Based on the RDF analysis, the PVC mixture exhibits significantly stronger van der Waals-type non-covalent interactions than the CPE mixture, as evidenced by the pronounced and sharper RDF peaks across multiple interaction sites. These findings align with the earlier discussion on hydrogen bonding, reinforcing the conclusion that the PVC blends have a stronger network of non-covalent interactions, which could influence the material properties of the blends.

Following the previous discussion, RDF analysis further identified weak C–H$\cdots\pi$ interactions between CPE/PVC and PM6 systems. Although weaker than the more prominent ones discussed earlier, these interactions still contribute to the non-covalent network that stabilizes the blend. Figures S2(a)–S2(e) illustrate the RDF peaks corresponding to C–H$\cdots\pi$ interactions between the methyl hydrogens ($m$-H) of CPE/PVC and the $\pi$-electron clouds of five- and six-membered rings. For PVC–PM6 blends, the RDF peaks reveal an average distance of around 5 Å, with a higher probability than CPE blends, as shown in Figs. S2(a) and S2(b). The broader peak widths observed in both cases suggest a range of distances where these interactions occur, likely due to the dynamic nature of molecular motions within the blend. Notably, in Fig. S2(c), PVC blends exhibit more C–H$\cdots\pi$ interactions, with the first RDF peak appearing at a distance of ~4.8 Å and a shoulder around

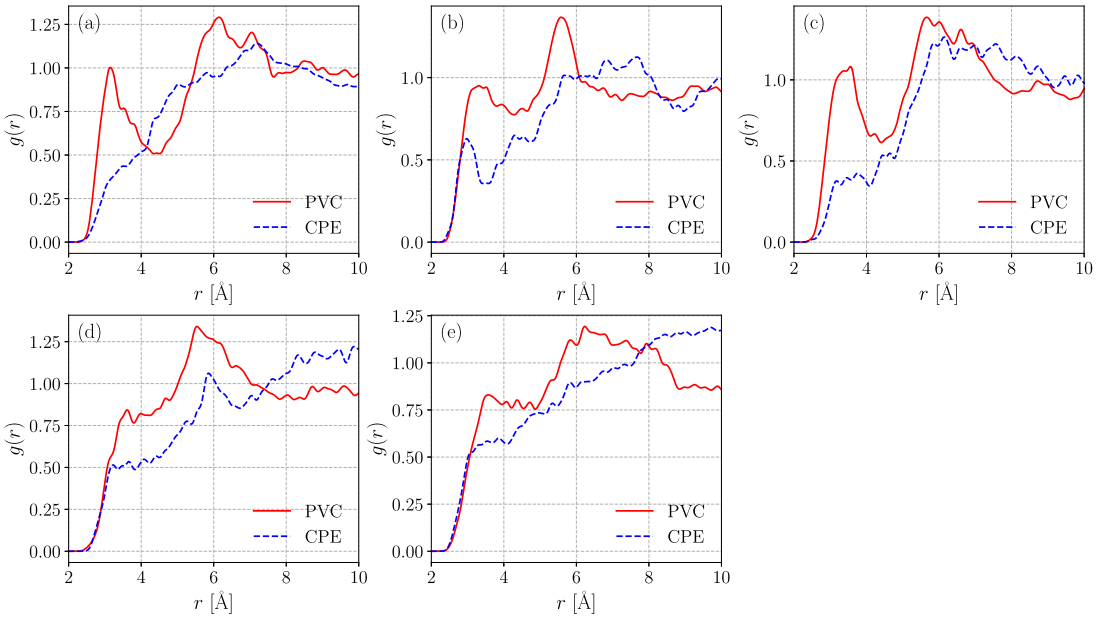


**FIG. 4.** RDF plots between $\pi$-cloud of the five-membered bridging ring, positioned between two five-membered rings fused with a six-membered ring in PM6 and (a) $\alpha-$ and (b) $\beta-$H of PVC/CPE molecules, respectively. (c) RDF corresponds to $\beta-$H and a five-member aromatic ring containing two methyl groups in PM6. RDF plots for C–H$\cdots\pi$ interactions between six-membered aromatic rings contain carbonyl groups in PM6 and (d) $\alpha-$ and (e) $\beta-$H of PVC/CPE molecules, respectively.

3.5 Å compared to other CPE blends, which display a slightly lower probability. In addition, Fig. S2(d) highlights a stronger C–H$\cdots\pi$ interaction in PVC blends, with the first peak observed around 4.75 Å, indicating a higher probability relative to CPE blends. Moreover, the enhanced intensity of the peaks in the PVC mixture, specifically for interactions involving five-membered rings, suggests that PVC engages in more robust C–H$\cdots\pi$ bonding than CPE.

The average distances observed for these interactions are larger than those identified earlier in Figs. 4(a)–4(e), which can be attributed to steric hindrance from the bulky methyl groups and the innermost rings. Despite the weaker nature of these interactions, their higher frequency in PVC blends compared to CPE blends implies a more stable and miscible system. This enhanced interaction network likely plays a role in preventing phase segregation over time, contributing to the long-term stability of the PVC–PM6 blend. Thus, even weak C–H$\cdots\pi$ interactions are crucial in maintaining the miscibility and structural integrity of the blend. This analysis reinforces the conclusion that the PVC–PM6 blends exhibit a more robust and diverse range of van der Waals-type interactions than the CPE–PM6 blends, further contributing to their superior stability and miscibility.

**C–Cl$\cdots\pi$ bonding:** Recent research has demonstrated that electronegative halogen atoms, typically considered electron donors due to their lone pairs, can also act as electron acceptors via the formation of $\sigma$-holes and $\pi$-holes.[51–54] This dual behavior allows halogens to participate in non-covalent interactions, significantly influencing molecular structure and properties. Previous studies have investigated the C–Cl$\cdots\pi$ interaction using infrared spectroscopy, complemented by theoretical methods such as Atoms in Molecules (AIMs) and Natural Bond Orbital (NBO) analysis. These studies revealed that C–Cl$\cdots\pi$ bonds are formed through both $\sigma$- and $\pi$-holes, with the $\sigma$-hole providing a stronger interaction compared to the $\pi$-hole.[55]

The current RDF analysis evaluated C–Cl$\cdots\pi$ interactions involving a five-membered aromatic ring with methyl groups. The results show that in PVC mixtures, the average distance for the first RDF peak is ~4.3 Å, shorter than the 4.8 Å observed in CPE mixtures [Fig. 5(a)]. Similarly, for interactions involving the six-membered ring system, the peak appears at 4.0 Å for PVC blends, compared to 4.9 Å for CPE blends [Fig. 5(b)]. Despite the shorter interaction distances in the PVC blends, the CPE mixtures exhibit a more prominent probability peak. Further analysis of the C–Cl$\cdots\pi$ interactions between chlorine atoms and the $\pi$-electron cloud of the five-membered bridging ring—situated between two fused five-membered rings—shows a particularly strong interaction in the PVC additive-conjugated polymer blends, with a peak at around 3.8 Å [Fig. 5(c)]. This suggests that the PVC system favors stronger non-covalent interactions involving chlorine, which could enhance the overall blend stability and miscibility compared to CPE mixtures.

In previous studies,[56,57] C–Cl stretching vibrations were observed in FTIR spectra due to C=O$\cdots$Cl–C interactions. Guan *et al.*[5] also observed similar C–Cl vibration spectra with FTIR spectra and attributed these vibrations to weak interactions between the carbon of the C=O group and chlorine in PVC linked to the isotactic arrangement of PM6 and PVC molecules. However, the present MD analysis reveals that these weak interactions are actually due to C–Cl$\cdots\pi$ interactions between the $\pi$ clouds of PM6 aromatic rings and the chlorine atoms in PVC/CPE molecules.

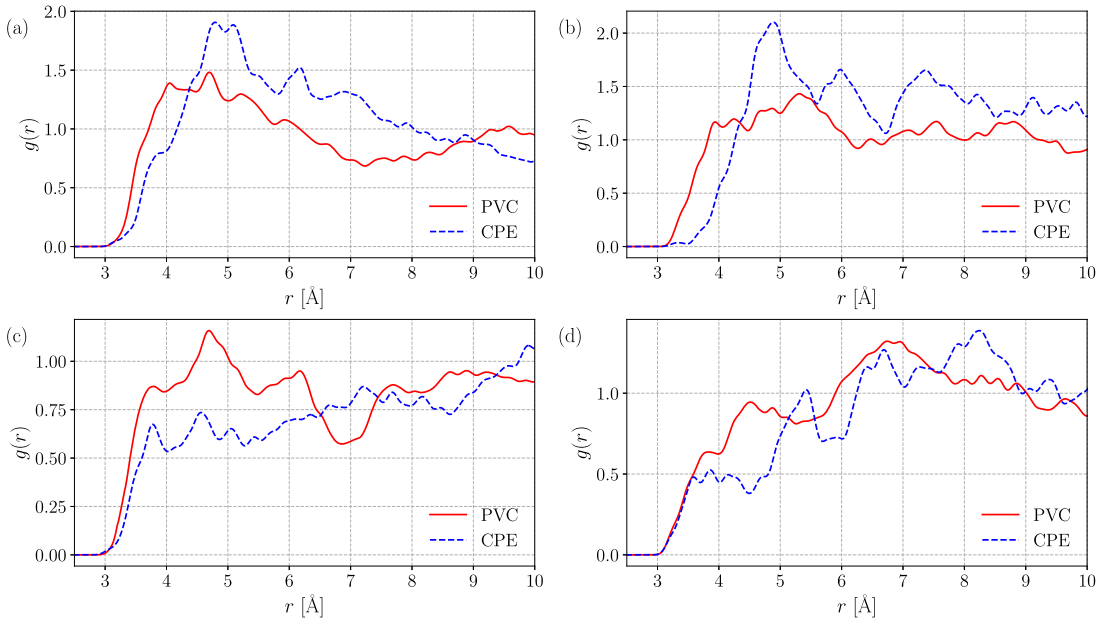


**FIG. 5.** Radial distribution function (RDF) plots representing C–Cl···$\pi$ interactions between the chlorine atoms of PVC/CPE molecules and the $\pi$-clouds of various regions within the PM6 structure: (a) the five-membered aromatic ring containing a single methyl group, (b) the five-membered aromatic ring containing two methyl groups, (c) the five-membered bridging ring located between two five-membered rings fused with a six-membered ring, and (d) the six-membered aromatic ring containing a carbonyl group.

**H···H bonding:** Following the analysis of van der Waals interactions, the discussion now shifts to the role of H···H bonding in the PVC/CPE and PM6 systems. These bonds, referred to as dihydrogen bonds, typically take the form $X^{\delta^-}$–$H^{\delta^+}$···$H^{\delta^-}$–$M^{\delta^+}$, where M represents a transition metal. Such interactions can arise from either intermolecular or intramolecular weak interactions. Short H···H contacts, typically in the range of 1.7–2.2 Å, have been identified in x-ray crystallographic studies of organometallic compounds[58] as well as in benzenoid systems.[59] Experimental and theoretical investigations of C–$H^{\delta^+}$···$H^{\delta^+}$–C interactions, modeled after the isotropic interaction potentials of $CH_4$ molecules, reveal bond energies around 0.4 kcal $mol^{-1}$.[60] Furthermore, closed-shell stabilizing interactions have been suggested between two hydrogen atoms carrying similar charges.[61]

In contrast to other weak interactions, the RDF analysis [Figs. S3(a)–S3(c)] did not show distinct peaks corresponding to H···H bonding across PVC/CPE blends. This indicates that the contribution of H···H interactions to the overall non-covalent interactions in these systems is minimal and can be considered negligible. This aligns with the earlier findings where van der Waals forces and C–H···$\pi$ interactions were the predominant contributors to the stability and miscibility of the PVC and CPE blends. Furthermore, the sparse distribution of PVC/CPE monomers within the PM6 matrix and the spatial separation of PM6's electron-accepting groups reduce the potential for cooperative effects among interactions. Consequently, the overall binding strength in these systems arises mainly from individual non-covalent interactions rather than cooperative contributions.

## C. NCI analysis

To further quantify the non-covalent interactions discussed previously, we employed non-covalent interaction index analysis. This approach uses peaks in the reduced density gradient (RDG) plot to indicate interference between atomic clouds, signaling the presence of non-covalent forces. The NCI method is enhanced by distinguishing between attractive and repulsive interactions through the sign of the second eigenvalue of the electron density Hessian matrix ($\lambda_2$). This distinction is critical, as it allows us to classify interactions based on the product of the sign of $\lambda_2$ and the electron density ($\rho$), denoted as (sign $\lambda_2$)$\rho$.[62] Repulsive interactions, often steric in nature, are represented by positive values of (sign $\lambda_2$)$\rho$, shown in red. In contrast, attractive interactions, such as van der Waals forces [with (sign $\lambda_2$)$\rho$ = 0] and hydrogen bonds [with (sign $\lambda_2$)$\rho$ < 0], are indicated by green and blue, respectively.[63] Visualizing RDG isosurfaces (Fig. 6) around their minima using the above-discussed coloring scheme reveals an intuitive representation of different interactions and their nature.

As shown in Fig. 7, the RDG trough plot reveals that PVC–PM6 blends show more pronounced attractive interactions—van der Waals and hydrogen bonds—compared to CPE–PM6 blends, as indicated by regions where sign($\lambda_2$)$\rho \leq 0$. To quantify these interactions, 100 configurations were extracted by selecting PM6 molecules within 6 Å of PVC or CPE molecules from the MD-simulated trajectory spanning 3 ns. This distance threshold allowed us to focus on configurations with direct non-covalent interactions. These selected configurations were then subjected to non-covalent interaction (NCI) analysis, which enabled us to visualize and quantify

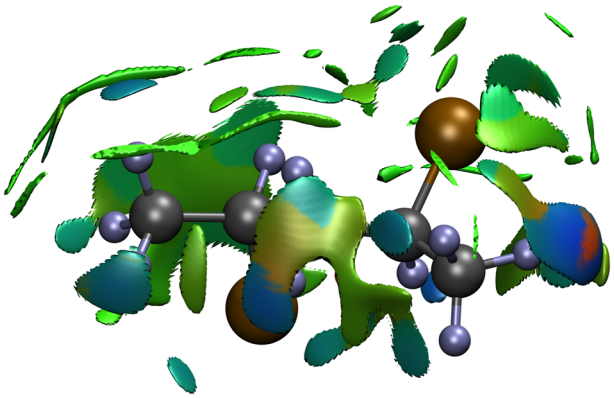

**FIG. 6.** Plot of isosurfaces of RDG(r) for a PVC–PM6 blend with a threshold value of 0.25, represented with a colored gradient based on the sign($\lambda_2$)$\rho$(r).

interaction regions based on the strength and nature of interactions. The analysis involved calculating the integrals of the global NCI density for regions characterized as strongly attractive, weak, or repulsive, as shown in Fig. S4. Following this systematic approach, we effectively transitioned from MD simulations to NCI analysis, isolating configurations with meaningful interaction profiles for detailed study.

This integration was performed across a range of signed electron density values [−0.1, 0.1 a.u.], allowing for a detailed classification of interaction types: strongly attractive interactions [−0.1 a.u. ≤ sign($\lambda_2$)$\rho$ < −0.02 a.u.], weak van der Waals interactions [−0.02 a.u. ≤ sign($\lambda_2$)$\rho$ ≤ 0.02 a.u.], and repulsive interactions [0.02 a.u. < sign($\lambda_2$)$\rho$ ≤ 0.1 a.u.]. The total integral values of these interactions were computed and plotted for different blends (see Fig. S4 of the supplementary material).

The tabulated data in Table I reveal the integrals of the global NCI density across different regions corresponding to the NCI analysis for the PM6–CPE and PM6–PVC blends. A smaller magnitude of integral density implies stronger non-covalent interactions (or binding force), and the data demonstrate that the PM6–PVC blend exhibits stronger interactions than the PM6–CPE blend. The evolution of integrals NCI density over MD trajectories for total and various interaction regions has been shown in Figs. S4(a)–S4(d). In the attractive region, the PM6–PVC blend has a slightly lower integral density value (0.000 89) than the PM6–CPE blend (0.001 14), indicating that the PVC blend experiences stronger attractive interactions. Similarly, in the van der Waals region, the PM6–PVC blend shows a lower integral density value (0.002 81) compared to the CPE blend (0.003 11), reinforcing the conclusion that the non-covalent van der Waals interactions are also more pronounced in the PVC blend.

**TABLE I.** Mean value of integral density in different regions corresponding to NCI analysis.

| Region | CPE | PVC |
|---|---|---|
| Attractive | 0.001 14 ± 0.000 06 | 0.000 89 ± 0.000 05 |
| van der Waals | 0.003 11 ± 0.000 07 | 0.002 81 ± 0.000 07 |
| Steric repulsion | 0.000 33 ± 0.000 02 | 0.000 23 ± 0.000 02 |
| Total | 0.004 59 ± 0.000 13 | 0.003 92 ± 0.000 12 |

The steric repulsion, which weakens interactions, is slightly higher in the PM6–PVC blend (0.000 23) than in the PM6–CPE blend (0.000 33). However, van der Waals interactions dominate over steric repulsion, contributing to a more tightly bound system overall in CPE and PVC blends. The total mean electron density is slightly lower for the PM6–PVC blend (0.0039) compared to the PM6–CPE blend (0.0046); this is indicative of stronger non-covalent interactions in the PVC system. The smaller value of total integral density suggests that, despite the slightly higher steric repulsion in PVC, the PM6–PVC blend benefits from a more optimal balance between attractive forces and repulsive interactions. Thus, the PM6–PVC blend exhibits stronger overall non-covalent interactions than the PM6–CPE blend, as reflected by the consistently lower integral density values across all regions. This enhanced interaction strength is likely to result in better stability and structural cohesion

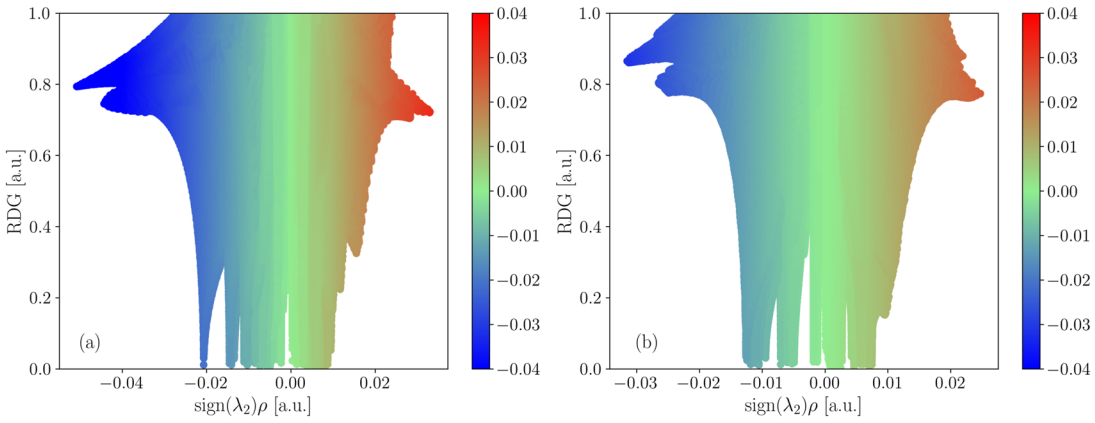


**FIG. 7.** Reduced gradient density plotted against sign($\lambda_2$)$\rho(r)$ for (a) PVC–PM6 and (b) CPE–PM6 mixtures.

in the PM6–PVC mixture. The integral density values are considerably small in regions of weak interactions, yet they account for a substantial portion of the overall interactions. Previous reports have shown that similar small integral density values correspond to a significant amount of binding energy.[64]

### D. Energy decomposition analysis

The energy decomposition analysis (EDA) offers valuable insights into the nature of the interactions within the PM6–CPE and PM6–PVC blends by breaking down the total interaction energy into its various components. This approach facilitates a deeper understanding of the driving forces behind the interaction and helps identify the primary contributors to the binding energy. Two main EDA approaches are commonly employed. Based on promolecular estimations, the first relies on variationally solved orbitals for individual fragments and the entire system. In this approach, the system's wavefunction is approximated as a Hartree product of the wavefunctions of the fragments. This method calculates individual energy contributions such as electrostatic, repulsion, and dispersion energies. From the promolecular-based EDA, we observe that the PVC blend exhibits stronger interactions compared to the CPE blend. In particular, the PVC blend has a lower total energy (−9.77 kJ/mol) than the CPE blend (−6.88 kJ/mol), indicating a higher binding energy in the PM6–PVC system.

The decomposition reveals that the dispersion contribution dominates, with values of −8.03 kJ/mol for the CPE blend and −11.17 kJ/mol for the PVC blend, suggesting that van der Waals interactions play a significant role in stabilizing the PVC blend. The electrostatic contributions, while smaller, also support this trend, with the PVC blend exhibiting a slightly more attractive electrostatic interaction (−1.38 kJ/mol) than the CPE blend (−1.07 kJ/mol). The repulsive interactions, on the other hand, are higher in the PVC blend (3.28 kJ/mol) compared to the CPE blend (2.33 kJ/mol), but their overall contribution remains minimal compared to attractive interactions.

To obtain a more accurate and nuanced view of these interactions, Symmetry-Adapted Perturbation Theory (SAPT) calculations were conducted. The results, shown in Table II, provide a more detailed decomposition of the interaction energies, including additional contributions such as induction, which captures the effects of polarization and dipole induction. The SAPT results further confirm the trends observed in the promolecular EDA. The total interaction energy for the PVC blend (−50.17 kJ/mol) is significantly lower than for the CPE blend (−39.00 kJ/mol), reinforcing the conclusion that the PVC blend is more strongly bound. Table II compares the contributions from electrostatic interactions alongside induction and dispersion interactions. The electrostatic interaction is particularly significant at larger intermolecular distances, affecting the overall interaction energy. For instance, the PVC blend exhibits lower electrostatic energy (−36.2768 kJ/mol) than the CPE blend (−27.8623 kJ/mol), highlighting its role in enhancing intermolecular binding and increased viscosity. The dispersion energy remains the dominant contributor, with the PVC blend exhibiting a stronger dispersion interaction (−68.67 kJ/mol) than the CPE blend (−64.92 kJ/mol). This is consistent with the stronger van der Waals interactions observed in the NCI analysis.

**TABLE II.** SAPT0 energy decomposition analysis for CPE/PM6 and PVC/PM6 blends, breaking down the total interaction energy into key components: electrostatics, exchange, induction, and dispersion.

| Decomposite energy (kJ/mol) | CPE | PVC |
|---|---|---|
| Electrostatics | −27.8623 | −36.2768 |
| Exchange | 59.6617 | 66.1714 |
| Induction | −5.8808 | −11.3965 |
| Dispersion | −64.9200 | −68.6660 |
| Total | −39.0015 | −50.1678 |

In addition, the SAPT results highlight the importance of induction in the PVC blend. The induction energy, which reflects polarization effects, is nearly twice as large in the PVC blend (−11.40 kJ/mol) compared to the CPE blend (−5.88 kJ/mol). This increased induction contribution suggests that the PVC blend experiences stronger dipole interactions, further enhancing its stability. In contrast, the exchange (repulsion) energy is higher for the PVC blend (66.17 kJ/mol) than for the CPE blend (59.66 kJ/mol), consistent with the trend observed in the promolecular EDA. However, the larger attractive contributions from dispersion and induction offset this increased repulsion, leading to a stronger overall interaction in the PVC blend.

In summary, the promolecular EDA and SAPT calculations consistently show that the PM6–PVC blend exhibits stronger non-covalent interactions than the PM6–CPE blend. The major contributors to this stronger binding are the enhanced dispersion and induction energies in the PVC blend, while repulsive interactions play a relatively minor role. These findings suggest that the PM6–PVC blend is likely more stable and exhibits better material properties than the PM6–CPE blend.

## IV. CONCLUSIONS

In conclusion, our study reveals that PVC/PM6 blends exhibit significantly greater stability compared to CPE/PM6 blends, largely due to the presence of stronger non-covalent interactions such as C–H$\cdots\pi$ and C–Cl$\cdots\pi$. These interactions are more pronounced in the PVC system, with the chlorine atom content playing a crucial role in facilitating stronger van der Waals and dipole interactions within the polymer matrix. The energy decomposition analysis (SAPT) supports this, indicating that PVC blends benefit from higher contributions from electrostatics and induction, further stabilizing the mixture.

Our findings suggest that additives with higher chlorine content tend to form more stable blends with conjugated polymers, making them promising candidates for applications where non-covalent interactions are critical for material performance. However, as the concentration of PVC increases, there is potential for phase segregation to occur, as intramolecular interactions within PVC may begin to dominate over intermolecular interactions. Future studies should explore the concentration limits at which these non-covalent interactions remain effective before phase segregation occurs, as well as strategies to mitigate this issue, such as adjusting blend ratios or introducing additional stabilizing components to maintain uniformity.

Overall, this work highlights the importance of understanding the balance between intermolecular forces and composition in designing stable polymer blends for advanced applications, with PVC showing great promise as a stabilizing additive.

## SUPPLEMENTARY MATERIAL

The supplementary material contains radial distribution functions.

## ACKNOWLEDGMENTS

The authors gratefully acknowledge the Indian Institute of Technology Gandhinagar, India, for providing the research facilities and financial support. R.S., R.K., and A.M. thank PARAM Ananta for the computational resources. A.M. acknowledges the SERB (Grant No. SRG/2022/001532) project for the funding.

## AUTHOR DECLARATIONS

### Conflict of Interest

The authors have no conflicts to disclose.

### Author Contributions

A.M. conceived the problem. R.S. and R.K. conducted all the simulations. R.S. and A.M. analyzed the results and prepared the draft.

**Ram Sewak**: Data curation (equal); Formal analysis (lead); Investigation (equal); Validation (equal); Visualization (equal); Writing – original draft (equal); Writing – review & editing (equal). **Rudranarayan Khatua**: Data curation (equal); Formal analysis (supporting); Investigation (supporting); Validation (supporting). **Anirban Mondal**: Conceptualization (lead); Formal analysis (equal); Funding acquisition (lead); Investigation (equal); Methodology (equal); Project administration (lead); Resources (lead); Supervision (lead); Validation (equal); Visualization (equal); Writing – original draft (lead); Writing – review & editing (lead).

## DATA AVAILABILITY

The data that support the findings of this study are available from the corresponding author upon reasonable request.

## REFERENCES

[1]A. G. S. Al-Azzawi, S. B. Aziz, E. M. A. Dannoun, A. Iraqi, M. M. Nofal, A. R. Murad, and A. M Hussein, "A mini review on the development of conjugated polymers: Steps towards the commercialization of organic solar cells," Polymers **15**, 164 (2022).
[2]X. Du, T. Heumueller, W. Gruber, O. Almora, A. Classen, J. Qu, F. He, T. Unruh, N. Li, and C. J. Brabec, "Unraveling the microstructure-related device stability for polymer solar cells based on nonfullerene small-molecular acceptors," Adv. Mater. **32**, 1908305 (2020).
[3]M. Ghasemi *et al.*, "A molecular interaction–diffusion framework for predicting organic solar cell stability," Nat. Mater. **20**, 525–532 (2021).
[4]J.-W. Lee *et al.*, "Establishing co-continuous network of conjugated polymers and elastomers for high-performance polymer solar cells with extreme stretchability," Adv. Energy Mater. **14**, 2401191 (2024).
[5]C. Guan, C. Xiao, X. Liu, Z. Hu, R. Wang, C. Wang, C. Xie, Z. Cai, and W. Li, "Non-covalent interactions between polyvinyl chloride and conjugated polymers enable excellent mechanical properties and high stability in organic solar cells," Angew. Chem., Int. Ed. **62**, e202312357 (2023).
[6]J. Zhang *et al.*, "Carboxylating elastomer via thiol-ene click reaction to improve miscibility with conjugated polymers for mechanically robust organic solar cells with efficiency of 19%," Adv. Mater. **36**, 2312805 (2024).
[7]C. Liu, C. Xiao, C. Xie, Q. Zhu, Q. Chen, W. Ma, and W. Li, "Insulating polymers as additives to bulk-heterojunction organic solar cells: The effect of miscibility," ChemPhysChem **23**, e202100725 (2022).
[8]Y. Kim *et al.*, "Enhanced charge injection properties of organic field-effect transistor by molecular implantation doping," Adv. Mater. **31**, 1806697 (2019).
[9]Z. Peng *et al.*, "Thermoplastic elastomer tunes phase structure and promotes stretchability of high-efficiency organic solar cells," Adv. Mater. **33**, 2106732 (2021).
[10]Q. Zhang, J. Huang, K. Wang, and W. Huang, "Recent structural engineering of polymer semiconductors incorporating hydrogen bonds," Adv. Mater. **34**, 2110639 (2022).
[11]L. A. Galuska, M. U. Ocheje, Z. C. Ahmad, S. Rondeau-Gagné, and X. Gu, "Elucidating the role of hydrogen bonds for improved mechanical properties in a high-performance semiconducting polymer," Chem. Mater. **34**, 2259–2267 (2022).
[12]Y. Wang, K.-L. Chen, A. Awada, N. Prine, Z. Cao, C. Zhu, Y.-C. Chiu, S. Rondeau-Gagné, and X. Gu, "Leveraging non-covalent interactions to control the morphology and electrical and mechanical properties of stretchable semiconducting composites," Chem. Mater. **35**, 9713–9724 (2023).
[13]M.-N. Chen *et al.*, "Facile blending strategy for boosting the conjugated polymer semiconductor transistor's mobility," ACS Appl. Mater. Interfaces **15**, 53755–53764 (2023).
[14]C. Xie, C. Xiao, X. Jiang, S. Liang, C. Liu, Z. Zhang, Q. Chen, and W. Li, "Miscibility-controlled mechanical and photovoltaic properties in double-cable conjugated polymer/insulating polymer composites," Macromolecules **55**, 322–330 (2022).
[15]P. A. Kollman, "Noncovalent interactions," Acc. Chem. Res. **10**, 365–371 (1977).
[16]K. Müller-Dethlefs and P. Hobza, "Noncovalent interactions: A challenge for experiment and theory," Chem. Rev. **100**, 143–168 (2000).
[17]A. S. Mahadevi and G. N. Sastry, "Cooperativity in noncovalent interactions," Chem. Rev. **116**, 2775–2825 (2016).
[18]P. Hobza and K. Müller-Dethlefs, *Non-Covalent Interactions: Theory and Experiment* (Royal Society of Chemistry, 2010).
[19]G. R. Desiraju and T. Steiner, "The weak hydrogen bond," in *Structural Chemistry and Biology* (Oxford University Press, 2001).
[20]P. A. Frey, S. A. Whitt, and J. B. Tobin, "A low-barrier hydrogen bond in the catalytic triad of serine proteases," Science **264**, 1927–1930 (1994).
[21]G. A. Jeffrey, *An Introduction to Hydrogen Bonding* (Oxford University Press, 1997).
[22]D. L. Howard and H. G. Kjaergaard, "Hydrogen bonding to divalent sulfur," Phys. Chem. Chem. Phys. **10**, 4113–4118 (2008).
[23]A. Chand, D. K. Sahoo, A. Rana, S. Jena, and H. S. Biswal, "The prodigious hydrogen bonds with sulfur and selenium in molecular assemblies, structural biology, and functional materials," Acc. Chem. Res. **53**, 1580–1592 (2020).
[24]J. Nadas, S. Vukovic, and B. P. Hay, "Alkyl chlorides as hydrogen bond acceptors," Comput. Theor. Chem. **988**, 75–80 (2012).
[25]W. L. Jorgensen, D. S. Maxwell, and J. Tirado-Rives, "Development and testing of the OPLS all-atom force field on conformational energetics and properties of organic liquids," J. Am. Chem. Soc. **118**, 11225–11236 (1996).
[26]W. L. Jorgensen and J. Tirado-Rives, "Potential energy functions for atomic-level simulations of water and organic and biomolecular systems," Proc. Natl. Acad. Sci. U. S. A. **102**, 6665–6670 (2005).

[27]B. Hess, C. Kutzner, D. van der Spoel, and E. Lindahl, "GROMACS 4: Algorithms for highly efficient, load-balanced, and scalable molecular simulation," J. Chem. Theory Comput. **4**, 435–447 (2008).
[28]S. Pronk *et al.*, "GROMACS 4.5: A high-throughput and highly parallel open source molecular simulation toolkit," Bioinformatics **29**, 845–854 (2013).
[29]L. S. Dodda, I. Cabeza de Vaca, J. Tirado-Rives, and W. L. Jorgensen, "LigParGen web server: An automatic OPLS-AA parameter generator for organic ligands," Nucleic Acids Res. **45**, W331–W336 (2017).
[30]M. J. Frisch *et al.*, Gaussian 09, Revision E.01, Gaussian, Inc., Wallingford, CT, 2009.
[31]L. Martínez, R. Andrade, E. G. Birgin, and J. M. Martínez, "PACKMOL: A package for building initial configurations for molecular dynamics simulations," J. Comput. Chem. **30**, 2157–2164 (2009).
[32]G. Bussi, D. Donadio, and M. Parrinello, "Canonical sampling through velocity rescaling," J. Chem. Phys. **126**, 014101 (2007).
[33]H. J. C. Berendsen, J. P. M. Postma, W. F. van Gunsteren, A. DiNola, and J. R. Haak, "Molecular dynamics with coupling to an external bath," J. Chem. Phys. **81**, 3684–3690 (1984).
[34]W. F. Van Gunsteren and H. J. C. Berendsen, "A leap-frog algorithm for stochastic dynamics," Mol. Simul. **1**, 173–185 (1988).
[35]W. Humphrey, A. Dalke, and K. Schulten, "VMD: Visual molecular dynamics," J. Mol. Graphics **14**, 33–38 (1996).
[36]R. A. Boto, F. Peccati, R. Laplaza, C. Quan, A. Carbone, J.-P. Piquemal, Y. Maday, and J. Contreras-García, "NCIPLOT4: Fast, robust, and quantitative analysis of noncovalent interactions," J. Chem. Theory Comput. **16**, 4150–4158 (2020).
[37]J. Contreras-García, E. R. Johnson, S. Keinan, R. Chaudret, J.-P. Piquemal, D. N. Beratan, and W. Yang, "NCIPLOT: A program for plotting noncovalent interaction regions," J. Chem. Theory Comput. **7**, 625–632 (2011).
[38]T. Lu, "A comprehensive electron wavefunction analysis toolbox for chemists, Multiwfn," J. Chem. Phys. **161**, 082503 (2024).
[39]D. G. A. Smith *et al.*, "PSI4 1.4: Open-source software for high-throughput quantum chemistry," J. Chem. Phys. **152**, 184108 (2020).
[40]J. F. Gonthier and C. D. Sherrill, "Density-fitted open-shell symmetry-adapted perturbation theory and application to $\pi$-stacking in benzene dimer cation and ionized DNA base pair steps," J. Chem. Phys. **145**, 134106 (2016).
[41]K. Patel, R. Khatua, K. Patrikar, and A. Mondal, "Exploring structure–property landscape of non-fullerene acceptors for organic solar cells," J. Chem. Phys. **160**, 144709 (2024).
[42]A. Mondal *et al.*, "Molecular library of OLED host materials—Evaluating the multiscale simulation workflow," Chem. Phys. Rev. **2**, 031304 (2021).
[43]N. B. Kotadiya, A. Mondal, P. W. M. Blom, D. Andrienko, and G.-J. A. H. Wetzelaer, "A window to trap-free charge transport in organic semiconducting thin films," Nat. Mater. **18**, 1182–1186 (2019).
[44]N. B. Kotadiya, A. Mondal, S. Xiong, P. W. M. Blom, D. Andrienko, and G.-J. A. H. Wetzelaer, "Rigorous characterization and predictive modeling of hole transport in amorphous organic semiconductors," Adv. Electron. Mater. **4**, 1800366 (2018).
[45]J. P. Wagner and P. R. Schreiner, "London dispersion in molecular chemistry—Reconsidering steric effects," Angew. Chem., Int. Ed. **54**, 12274–12296 (2015).
[46]A. M. Reilly and A. Tkatchenko, "van der Waals dispersion interactions in molecular materials: beyond pairwise additivity," Chem. Sci. **6**, 3289–3301 (2015).
[47]J. Hwang, P. Li, M. D. Smith, and K. D. Shimizu, "Distance-dependent attractive and repulsive interactions of bulky alkyl groups," Angew. Chem., Int. Ed. **55**, 8086–8089 (2016).
[48]J. Echeverría, G. Aullón, D. Danovich, S. Shaik, and S. Alvarez, "Dihydrogen contacts in alkanes are subtle but not faint," Nat. Chem. **3**, 323–330 (2011).
[49]M. Nishio, Y. Umezawa, J. Fantini, M. S. Weiss, and P. Chakrabarti, "CH-$\pi$ hydrogen bonds in biological macromolecules," Phys. Chem. Chem. Phys. **16**, 12648–12683 (2014).
[50]S. Tsuzuki, "CH/$\pi$ interactions," Annu. Rep. Prog. Chem., Sect. C:Phys. Chem. **108**, 69–95 (2012).
[51]A. Mohajeri, A. H. Pakiari, and N. Bagheri, "Theoretical studies on the nature of bonding in $\sigma$-hole complexes," Chem. Phys. Lett. **467**, 393–397 (2009).
[52]P. Politzer, J. S. Murray, and T. Clark, "Halogen bonding: An electrostatically-driven highly directional noncovalent interaction," Phys. Chem. Chem. Phys. **12**, 7748–7757 (2010).
[53]J. S. Murray, P. Lane, T. Clark, K. E. Riley, and P. Politzer, "$\sigma$-holes, $\pi$-holes and electrostatically-driven interactions," J. Mol. Model. **18**, 541–548 (2012).
[54]J. E. D. Bene, I. Alkorta, and J. Elguero, "Properties of complexes $H_2C{=}(X)P{:}PXH_2$, for X = F, Cl, OH, CN, NC, CCH, H, $CH_3$, and $BH_2$: P···P pnicogen bonding at σ-holes and π-holes," J. Phys. Chem. A **117**, 11592–11604 (2013).
[55]N. Ramanathan, K. Sundararajan, K. Vidya, and E. D. Jemmis, "Non-covalent C–Cl. . .$\pi$ interaction in acetylene-carbon tetrachloride adducts: Matrix isolation infrared and *ab initio* computational studies," Spectrochim. Acta, Part A **157**, 69–78 (2016).
[56]H. J. Salavagione, G. Ellis, and G. Martínez, "Poly(vinyl chloride)/multiwalled carbon nanotube nanocomposites: Effect of the tacticity distribution on the polymer/nanofiller interface," J. Phys. Chem. C **116**, 18256–18262 (2012).
[57]D. L. Tabb and J. L. Koenig, "Fourier transform infrared study of plasticized and unplasticized poly(vinyl chloride)," Macromolecules **8**, 929–934 (1975).
[58]D. J. Wolstenholme and T. S. Cameron, "Comparative study of weak interactions in molecular crystals: H–H bonds vs hydrogen bonds," J. Phys. Chem. A **110**, 8970–8978 (2006).
[59]J. Cioslowski and S. T. Mixon, "Universality among topological properties of electron density associated with the hydrogen–hydrogen nonbonding interactions," Can. J. Chem. **70**, 443–449 (1992).
[60]J. J. Novoa, M. Whangbo, and J. M. Williams, "Interactions energies associated with short intermolecular contacts of C–H bonds. II. *Ab–initio* computational study of the C–H· · ·H–C interactions in methane dimer," J. Chem. Phys. **94**, 4835–4841 (1991).
[61]C. F. Matta, J. Hernández-Trujillo, T.-H. Tang, and R. F. W. Bader, "Hydrogen–hydrogen bonding: A stabilizing interaction in molecules and crystals," Chem. - Eur. J. **9**, 1940–1951 (2003).
[62]N. S. Venkataramanan, A. Suvitha, and Y. Kawazoe, "Intermolecular interaction in nucleobases and dimethyl sulfoxide/water molecules: A DFT, NBO, AIM and NCI analysis," J. Mol. Graphics Modell. **78**, 48–60 (2017).
[63]E. R. Johnson, S. Keinan, P. Mori-Sánchez, J. Contreras-García, A. J. Cohen, and W. Yang, "Revealing noncovalent interactions," J. Am. Chem. Soc. **132**, 6498–6506 (2010).
[64]E. K. Wieduwilt, R. A. Boto, G. Macetti, R. Laplaza, J. Contreras-García, and A. Genoni, "Extracting quantitative information at quantum mechanical level from noncovalent interaction index analyses," J. Chem. Theory Comput. **19**, 1063–1079 (2023).